Terahertz Signal Classification Based on Geometric Algebra

Shengling Zhou, Dimitar G. Valchev, Alex Dinovitser, *Member, IEEE*, James M. Chappell, Azhar Iqbal, Brian Wai-Him Ng, *Member, IEEE*, Tak W. Kee, and Derek Abbott, *Fellow, IEEE*

***Abstract*—This paper presents an approach to classification of substances based on their terahertz spectra. We use geometric algebra to provide a concise mathematical means for attacking the classification problem in a coordinate-free form. For the first time, this allows us to perform classification independently of dispersion and, hence, independently of the transmission path length through the sample. Finally, we validate the approach with experimental data. In principle, the coordinate-free transformation can be extended to all types of pulsed signals, such as pulsed microwaves or even acoustic signals in the field of seismology. Our source code for classification based on geometric algebra is publicly available at: https://github.com/swuzhousl/Shengling-zhou/blob/geometric-algebra-classifier/GAclassifier/.**

***Index Terms*—Classification, geometric algebra, multivectors, spectroscopy, terahertz (THz).**

I. Introduction

TERAHERTZ (THz) inspection systems can penetrate common packaging materials and provide substance detection of the contents by measuring the complex refractive index of materials over a wide range of frequencies [1], [2]. The identification of different substances can be achieved via adoption of a signal classifier that is trained to discriminate absorption spectra in the THz regime [3].

In a general application where there may be little or no *a priori* knowledge of the target, it becomes advantageous to capture THz spectra both in reflection and in transmission simultaneously. Dual THz systems that perform simultaneous transmission and reflection measurements have been developed [4]. Reflective measurements avoid the disadvantages of transmission; however, this is at the expense of a signal scattered over a wide capture angle, thereby reducing the signal-to-noise ratio (SNR). Transmission measurements offer improved collimation of energy; however, SNR will rapidly fall off as a function of the thickness of the sample. Thus, in practice, a dual reflection and transmission mode system assists in maximizing the total information that can be obtained from an arbitrary sample.

A problem with using pulsed terahertz time-domain spectroscopy (THz-TDS) systems is the dispersion of the THz pulse through the sample. This dispersion results in temporal pulse spreading, and therefore classifiers trained on a substance of a given thickness do not generalize. In other words, if a signal classifier has been trained using both frequency and phase data for a sample of one thickness, it may not always work for a target sample of a different thickness. Clearly, retraining the classifier for every expected substance thickness is highly impractical.

A standard solution to this problem is to move away from pulsed systems and turn to THz continuous wave (CW) systems [5], thus avoiding the issue of pulse dispersion in the first place—but this is at the expense of direct capture of phase information. On the other hand, a pulsed THz-TDS system is desirable as it rapidly captures many frequencies, and chirped systems even offer one-shot capture [6]. Also due to the high pulse powers, pulsed systems offer a higher dynamic range over CW counterparts [7].

Thus, the key question we address in this paper is: Can classification of THz pulses in transmission be carried out in a dispersion independent manner? If this can be achieved, then dual reflection and transmission pulsed THz inspection systems will have a much wider practical application space.

The approach we take in this paper is to essentially find a higher dimensional mathematical space over which all THz pulses lie on the same hyperplane if they represent a unique substance, independent of the dispersion. In other words, we find a mathematical projection that enables us to perform dispersion-independent signal classification.

Geometric algebra (GA) is the most convenient mathematical framework for handling higher dimensional spaces. It has already been successfully applied to complex signal [8] and image processing [9], computer vision [10], electrical engineering [11], etc. Following the approach in [12], we briefly introduce this methodology and, second, we show how it may be

Manuscript received April 26, 2016; revised July 19, 2016; accepted September 6, 2016. Date of publication October 12, 2016; date of current version November 1, 2016. This work was supported by the National key R&D program of China under Grant 2016YFC0502301, by the Fundamental Research Funds for the Central Universities under Program XDJK2014c132, and by the Australian Research Council under Grant FT120100351. The work of D. G. Valchev was supported by the Group of Eight 2014 European Fellowship scheme. The work of S. Zhou was supported by the 2015 China Scholarship Council scheme.

S. Zhou is with the School of Engineering and Technology, Southwest University, Chongqing 400715, China, and also with the Department of Chemistry, School of Physical Sciences and the School of Electrical and Electronic Engineering, The University of Adelaide, Adelaide, SA 5005, Australia (e-mail: swuzhousl@163.com).

D. G. Valchev is with the Department of Computer Systems and Technologies, University of Food Technologies, Plovdiv 4000, Bulgaria, and also with the School of Electrical and Electronic Engineering, The University of Adelaide, Adelaide, SA 5005, Australia (e-mail: dimitar.valchev@gmail.com).

A. Dinovitser, J. M. Chappell, A. Iqbal, B. W.-H. Ng, and D. Abbott are with the School of Electrical and Electronic Engineering, The University of Adelaide, Adelaide, SA 5005, Australia (e-mail: alex.dinovitser@gmail.com; jamie2007@mail.com; mr.azhariqbal@gmail.com; brian.ng@adelaide.edu.au; derek.abbott@adelaide.edu.au).

T. W. Kee is with the Department of Chemistry, School of Physical Sciences, The University of Adelaide, Adelaide, SA 5005, Australia (e-mail: tak.kee@adelaide.edu.au).

Color versions of one or more of the figures in this paper are available online at http://ieeexplore.ieee.org.

Digital Object Identifier 10.1109/TTHZ.2016.2610759

used for isolating dispersion-independent hyperplanes in higher dimensions.

Next, we perform THz-TDS measurements on a number of substances of varying thicknesses. We then use these data to validate the approach by comparing the performance of GA classification with the performance of a conventional support vector machine (SVM) classifier. The reason we select the SVM classifier for comparison is that it has been previously demonstrated as one of the most robust and accurate for THz-TDS signals [13], [14].

Our original contribution is that for the first time we theoretically demonstrate that a classifier based on GA is nearly independent of signal dispersion in the ideal noise-free case. Moreover, in the nonideal case, we experimentally demonstrate reduced dependence on dispersion.

A. Brief Introduction to GA

Clifford GA $C\ell\left(\Re^n\right)$ represents an associative graded real algebra over n dimensions. We can define the algebra through selecting a set of basis vectors $\{e_1, \ldots, e_n\}$, where we specify $e_i^2 = 1, i = 1, 2, \ldots, n$, with the basis elements e_i anticommuting with each other. The scalars, vectors e_i, bivectors $e_i e_j$, trivectors $e_i e_j e_k$, etc., formed from distinct basis vectors form the grades of the algebra from 0 to n, respectively. We write a general vector $\boldsymbol{v} = v_1 e_1 + v_2 e_2 + \cdots + v_n e_n$, where $v_1, v_2, \ldots, v_n$ are real scalars that, using the rules of the algebra, give the product $\boldsymbol{v}^2 = v_1^2 + v_2^2 + \cdots + v_n^2$, where we assume the distribution of multiplication over addition when expanding brackets. For two vectors we can form the geometric product as

$$\boldsymbol{v}\boldsymbol{w} = \frac{1}{2}\left(\boldsymbol{v}\boldsymbol{w} + \boldsymbol{w}\boldsymbol{v}\right) + \frac{1}{2}\left(\boldsymbol{v}\boldsymbol{w} - \boldsymbol{w}\boldsymbol{v}\right) = \boldsymbol{v}\cdot\boldsymbol{w} + \boldsymbol{v}\wedge\boldsymbol{w}. \tag{1}$$

That is, $\boldsymbol{v}\cdot\boldsymbol{w} = \frac{1}{2}\left(\boldsymbol{v}\boldsymbol{w} + \boldsymbol{w}\boldsymbol{v}\right)$ and $\boldsymbol{v}\wedge\boldsymbol{w} = \frac{1}{2}\left(\boldsymbol{v}\boldsymbol{w} - \boldsymbol{w}\boldsymbol{v}\right)$, which corresponds with the conventional definitions of the dot and wedge products [15]. In three dimensions, the wedge product corresponds with the conventional vector cross product. Note that the wedge product is anticommuting so that $\boldsymbol{v}\wedge\boldsymbol{w} = -\boldsymbol{w}\wedge\boldsymbol{v}$ and consists of a linear combination of bivector elements $e_i e_j$. The special case of bivectors formed from the wedge product of two vectors is referred to as a 2-blade. In general, we define an r-blade as an outer product of r linearly independent vectors. The wedge product $\boldsymbol{v}\wedge\boldsymbol{w}$ geometrically describes an oriented plane in n dimensions, where the vectors $\boldsymbol{v}$ and $\boldsymbol{w}$ lie in this plane. Fig. 1 shows how a plane is described by a 2-blade $\boldsymbol{H}$ formed from two vectors $\boldsymbol{f}$ and $\boldsymbol{\alpha}$. Due to their importance, we specifically denote 2-blades with bold uppercase letters, for example, $\boldsymbol{B} = \boldsymbol{v}\wedge\boldsymbol{w}$. Vectors are then distinguished by using lowercase bold symbols. For a third vector $\boldsymbol{x}$, we can then form the 3-blade $\boldsymbol{B}\wedge\boldsymbol{x} = \boldsymbol{v}\wedge\boldsymbol{w}\wedge\boldsymbol{x}$. If this 3-blade (representing an oriented volume) is zero, then the vectors must be coplanar [16]–[18]. We also have the highest grade element given by $j = e_1 e_2 \ldots e_n$, where by selecting n appropriately, we have $j^2 = -1$ that commutes with all other elements of the algebra. These properties of j imply that it can be treated in the same way as the scalar unit imaginary $\sqrt{-1}$.

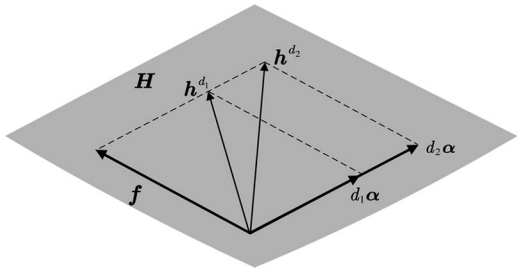

Fig. 1. The substance 2-blade (plane) $\boldsymbol{H}$, in $2m$ dimensions, is defined by the pair of vectors $\boldsymbol{f}$ and $\boldsymbol{\alpha}$, with experimental measurements $\boldsymbol{h}^{d_1}$ and $\boldsymbol{h}^{d_2}$ also lying in this plane, from (9).

We use the notation $\tilde{h} = a + jb, a, b \in \Re$ to identify situations where we are dealing with complex-like numbers that include the n-blade j. We also denote complex-like vectors with similar notation $\tilde{\boldsymbol{h}} = \boldsymbol{v} + j\boldsymbol{w}$. Naturally, the operators Re and Im now refer to the real- and imaginary-like (represented by j) parts of these numbers.

II. Correspondence of a THz Measurement to a 2-Blade

In a THz-TDS setting, two signals in the time domain are recorded: a signal through the propagation medium (usually free space), termed the reference THz signal, and a signal through the sample, termed the sample THz signal. These two signals are then Fourier transformed for obtaining their corresponding spectra. Dividing the spectrum from the sample $E_{\mathrm{sam}}(\omega)$ by the reference spectrum $E_{\mathrm{ref}}(\omega)$, the complex-valued transfer function $\tilde{h}(\omega)$ for the target substance is obtained as follows:

$$\begin{aligned}\tilde{h}(\omega) &= \frac{E_{\mathrm{sam}}(\omega)}{E_{\mathrm{ref}}(\omega)} = \frac{4\tilde{n}(\omega) n_m}{\left[\tilde{n}(\omega) + n_m\right]^2} \exp\left\{-\kappa(\omega)\frac{\omega d}{c}\right\} \\ &\quad \times \exp\left\{-j\left[n(\omega) - n_m\right]\frac{\omega d}{c}\right\}\end{aligned} \tag{2}$$

where c is the speed of light in vacuum, ω is the angular frequency, d is the sample thickness, $\tilde{n}(\omega) = n(\omega) - j\kappa(\omega)$ is the frequency-dependent complex refractive index of the sample, and n_m is the refractive index of the propagation medium. The real and imaginary components of the complex refractive index of the sample are, respectively, the refractive index $n(\omega)$ and the extinction coefficient $\kappa(\omega)$ of the sample. These two components can be obtained, respectively, from the phase and the amplitude of the complex-valued transfer function $\tilde{h}(\omega)$ in (2). It can be seen that the phase angle of this transfer function is expressed as

$$\angle\tilde{h}(\omega) = \angle\frac{4\tilde{n}(\omega) n_m}{\left[\tilde{n}(\omega) + n_m\right]^2} - \left[n(\omega) - n_m\right]\frac{\omega d}{c}. \tag{3}$$

Also, the natural logarithm of the magnitude of the transfer function is expressed as

$$\ln\left|\tilde{h}(\omega)\right| = \ln\left|\frac{4\tilde{n}(\omega) n_m}{\left[\tilde{n}(\omega) + n_m\right]^2}\right| - \kappa(\omega)\frac{\omega d}{c}. \tag{4}$$

The $\frac{4\tilde{n}(\omega)n_m}{[\tilde{n}(\omega)+n_m]^2}$ term is the Fresnel loss at the sample-medium interfaces and can be denoted as $\tilde{f}(\omega)$.

Due to the nature of the THz-TDS system, with the use of a discrete Fourier transform, all the presented functions of frequency are sampled at frequencies ω_i with $i = 1, 2, \ldots, m$. Thus, the complex refractive index $\tilde{n}(\omega)$, the complex transfer function $\tilde{h}(\omega)$, and the complex Fresnel loss $\tilde{f}(\omega)$ are expressed, respectively, by the m-dimensional vectors $\tilde{\boldsymbol{n}}$, $\tilde{\boldsymbol{h}}$, and $\tilde{\boldsymbol{f}}$. Since these three vectors are complex valued, each of them contains $2m$ real values. Two functions, $\boldsymbol{g}_1(\cdot)$ and $\boldsymbol{g}_2(\cdot)$, are defined for mapping these m-dimensional complex-valued vectors to $2m$-dimensional real-valued vectors. For a set of $2m$ orthonormal basis vectors $\boldsymbol{e}_i, i = 1, 2, \ldots, 2m$, and an arbitrary m-dimensional complex-valued vector $\tilde{\boldsymbol{v}}$ with components $\tilde{v}_i, i = 1, 2, \ldots, m$, these two functions are defined as follows:

$$\boldsymbol{g}_1(\tilde{\boldsymbol{v}}) = \sum_{i=1}^{m} \mathrm{Re}(\tilde{v}_i)\,\boldsymbol{e}_i + \sum_{i=1}^{m} \mathrm{Im}(\tilde{v}_i)\,\boldsymbol{e}_{i+m}, \tag{5}$$

$$\boldsymbol{g}_2(\tilde{\boldsymbol{v}}) = \sum_{i=1}^{m} \angle\tilde{v}_i \boldsymbol{e}_i + \sum_{i=1}^{m} \ln|\tilde{v}_i|\,\boldsymbol{e}_{i+m}. \tag{6}$$

Applying the function $\boldsymbol{g}_2(\cdot)$ to the m-dimensional complex-like vector $\tilde{\boldsymbol{h}}$, the $2m$-dimensional real vector $\boldsymbol{h}$ is obtained as

$$\boldsymbol{g}_2\left(\tilde{\boldsymbol{h}}\right) = \boldsymbol{h} = \sum_{i=1}^{m} \angle\tilde{h}_i \boldsymbol{e}_i + \sum_{i=1}^{m} \ln\left|\tilde{h}_i\right| \boldsymbol{e}_{i+m}. \tag{7}$$

An m-dimensional vector $\tilde{\boldsymbol{\alpha}}$ now is defined with its m components being $\tilde{\alpha}_i = -(n_i - n_m + j\kappa_i)\frac{\omega_i}{c}, i = 1, 2, \ldots, m$. Then from (7), using (3) and (4), $\boldsymbol{h}$ is obtained as

$$\begin{aligned}
\boldsymbol{h} = & \sum_{i=1}^{m} \left\{ \angle\tilde{h}_i - [n_i - n_m]\frac{\omega_i d}{c} \right\} \boldsymbol{e}_i \\
& + \sum_{i=1}^{m} \left[\ln\left|\tilde{f}_i\right| - \frac{\kappa_i \omega_i d}{c} \right] \boldsymbol{e}_{i+m} \\
= & \sum_{i=1}^{m} \angle\tilde{f}_i \boldsymbol{e}_i + \sum_{i=1}^{m} \ln\left|\tilde{f}_i\right| \boldsymbol{e}_{m+i} \\
& + \sum_{i=1}^{m} \left\{ -[n_i - n_m]\frac{\omega_i d}{c} \right\} \boldsymbol{e}_i + \sum_{i=1}^{m} \left[-\frac{\kappa_i \omega_i d}{c} \right] \boldsymbol{e}_{i+m} \\
= & \sum_{i=1}^{m} \angle\tilde{f}_i \boldsymbol{e}_i + \sum_{i=1}^{m} \ln\left|\tilde{f}_i\right| \boldsymbol{e}_{m+i} \\
& + d\sum_{i=1}^{m} \mathrm{Re}(\tilde{\alpha}_i)\,\boldsymbol{e}_i + d\sum_{i=1}^{m} \mathrm{Im}(\tilde{\alpha}_i)\,\boldsymbol{e}_{i+m}.
\end{aligned} \tag{8}$$

After the last equality of (8), the first two terms can be identified as $\boldsymbol{g}_2(\tilde{\boldsymbol{f}})$ through (6) and the last two terms can be identified as $d\boldsymbol{g}_1(\tilde{\boldsymbol{\alpha}})$ through (5). Therefore, $\boldsymbol{g}_2(\tilde{\boldsymbol{h}}) = \boldsymbol{g}_2(\tilde{\boldsymbol{f}}) + d\boldsymbol{g}_1(\tilde{\boldsymbol{\alpha}})$. Denoting $\boldsymbol{\alpha} = \boldsymbol{g}_1(\tilde{\boldsymbol{\alpha}})$ and $\boldsymbol{f} = \boldsymbol{g}_2(\tilde{\boldsymbol{f}})$, (8) reduces to

$$\boldsymbol{h} = \boldsymbol{f} + d\boldsymbol{\alpha}. \tag{9}$$

In (9), the first term corresponds to the Fresnel loss and the second term corresponds to the complex refractive index of the target substance. This expression shows that the measured THz spectrum for the substance (the m-dimensional complex-valued vector $\tilde{\boldsymbol{h}}$ of the transfer function) can be transformed into a $2m$-dimensional vector $\boldsymbol{h}$, which is a sum of a $2m$-dimensional vector $\boldsymbol{f}$ determined by the Fresnel loss and a scaled $2m$-dimensional vector $\boldsymbol{\alpha}$ determined by the complex refractive index. The second term of the sum in (9) depends *linearly* on the sample thickness d. The vectors $\boldsymbol{f}$ and $\boldsymbol{\alpha}$ are not parallel and therefore linearly independent of each other or, in terms of GA, $\boldsymbol{f} \wedge \boldsymbol{\alpha} \neq 0$.

It is assumed that for any two different substances A and B, their corresponding complex refractive indices, $\tilde{\boldsymbol{n}}_A$ and $\tilde{\boldsymbol{n}}_B$, are neither linearly dependent, nor the complex conjugate of each other. In terms of GA, linear independence requires that

$$\boldsymbol{f}_A \wedge \boldsymbol{\alpha}_A \wedge \boldsymbol{f}_B \wedge \boldsymbol{\alpha}_B \neq 0. \tag{10}$$

Based on these assumptions, the following theorems can be easily proved (see Appendix).

Theorem 1: Each vector $\tilde{\boldsymbol{n}}$ of a complex refractive index determines unique vectors $\tilde{\boldsymbol{f}}$ and $\tilde{\boldsymbol{\alpha}}$ (hence, unique vectors $\boldsymbol{f}$ and $\boldsymbol{\alpha}$), and vice versa.

Theorem 2: Each complex refractive index vector $\tilde{\boldsymbol{n}}$ determines in the $2m$-dimensional space a unique unit 2-blade $\boldsymbol{H} = \frac{\boldsymbol{f}\wedge\boldsymbol{\alpha}}{|\boldsymbol{f}\wedge\boldsymbol{\alpha}|}$.

Theorem 3: All vectors $\boldsymbol{h}^d = \boldsymbol{f} + d\boldsymbol{\alpha}\,(\forall d \in R)$ are coplanar and belong to the hyperplane $\boldsymbol{H}$.

Theorem 2 shows that each substance under investigation corresponds to a unique 2-blade in the $2m$-dimensional multivector space of measured THz spectra, transformed through (9). Theorem 3 shows that samples of one substance but with different thicknesses belong to the same 2-blade determined by the substance according to Theorem 2. Therefore, the same 2-blade can be determined by two vectors, $\boldsymbol{h}^{d_1}$ and $\boldsymbol{h}^{d_2}$, obtained through measurements of samples of two different thicknesses, d_1 and d_2, of the same substance as

$$\begin{aligned}
\boldsymbol{h}^{d_1} \wedge \boldsymbol{h}^{d_2} &= (\boldsymbol{f} + d_1\boldsymbol{\alpha}) \wedge (\boldsymbol{f} + d_2\boldsymbol{\alpha}) \\
&= \boldsymbol{f} \wedge \boldsymbol{f} + d_2\boldsymbol{f} \wedge \boldsymbol{\alpha} + d_1\boldsymbol{\alpha} \wedge \boldsymbol{f} + d_1\boldsymbol{\alpha} \wedge d_2\boldsymbol{\alpha}.
\end{aligned} \tag{11}$$

As the first and last terms in (11) vanish, we obtain

$$\boldsymbol{h}^{d_1} \wedge \boldsymbol{h}^{d_2} = (d_2 - d_1)(\boldsymbol{f} \wedge \boldsymbol{\alpha}) = \Delta d(\boldsymbol{f} \wedge \boldsymbol{\alpha}) \tag{12}$$

with $\Delta d = (d_2 - d_1)$ being the difference in thicknesses of the two samples of the same substance. It is seen that the vector pair $\boldsymbol{h}^{d_1}$ and $\boldsymbol{h}^{d_2}$ determines the same 2-blade as the vector pair $\boldsymbol{f}$ and $\boldsymbol{\alpha}$, up to a scaling constant. Therefore, the unit 2-blade is

$$\boldsymbol{H} = \frac{\boldsymbol{f} \wedge \boldsymbol{\alpha}}{|\boldsymbol{f} \wedge \boldsymbol{\alpha}|} = \frac{\boldsymbol{h}^{d_1} \wedge \boldsymbol{h}^{d_2}}{\left|\boldsymbol{h}^{d_1} \wedge \boldsymbol{h}^{d_2}\right|} \tag{13}$$

where (13) will be used for determining the 2-blade corresponding to the THz measurement data in Section IV. For any substance under investigation, its corresponding vectors $\boldsymbol{f}$ and $\boldsymbol{\alpha}$

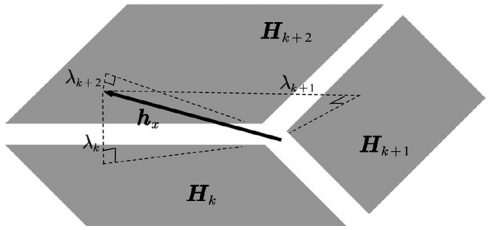

Fig. 2. The measurement vector $\boldsymbol{h}_x$ along with 2-blades (planes) corresponding to three substances, $\boldsymbol{H}_k$, $\boldsymbol{H}_{k+1}$, and $\boldsymbol{H}_{k+2}$, in $2m$ dimensions. The closer the measurement vector is to a particular 2-blade, the lower the value of λ is and the more likely the measured unknown substance with an unknown sample thickness is the substance corresponding to that 2-blade. Here, the substance corresponding to the 2-blade $\boldsymbol{H}_{k+2}$ is most likely the one corresponding also to the measurement vector $\boldsymbol{h}_x$.

are generally *a priori* unknown. But the measured vectors $\boldsymbol{h}^{d_1}$ and $\boldsymbol{h}^{d_2}$ determine the *same* 2-blade as illustrated in Fig. 1.

Once the set of all planes for the different substances under investigation is determined within the $2m$-dimensional space, the measurement of the THz spectrum of an unknown substance x with an unknown sample thickness can take place, producing a measurement vector $\boldsymbol{h}_x$. This vector is then checked for belonging to the planes of all the N different 2-blades of possible substances, assuming that the unknown substance is the same as one of the corresponding 2-blades.

This is significant given that the signal is affected by inevitable noise and other factors in a THz-TDS system, so the vectors will deviate from their original orientation and move away from the planes. To estimate this deviation, the magnitude rejection[1] of the vector to the plane is given by the parameter λ. This parameter is defined as

$$\lambda = \left| \frac{\boldsymbol{h}_x}{|\boldsymbol{h}_x|} \wedge \boldsymbol{H} \right|, \quad 0 \leq \lambda \leq 1. \tag{14}$$

The closer the vector is to the plane, the lower the value of λ. In the ideal case, the value of λ is equal to zero.

Therefore, a substance identification method based on the minimum value of the parameter λ is presented as

$$\begin{aligned} x &= \arg\min_k \{\lambda_k\} \\ &= \arg\min_k \left| \frac{\boldsymbol{h}_x}{|\boldsymbol{h}_x|} \wedge \boldsymbol{H}_k \right|, \quad k = 1, 2, \ldots, N. \end{aligned} \tag{15}$$

The plane with the minimum value of λ with the measurement vector $\boldsymbol{h}_x$ is most likely the plane of the unknown measured substance. The measurement vector $\boldsymbol{h}_x$ along with three planes representing different substances is illustrated in Fig. 2.

III. Dispersion and Noise

In order to explore the influence of dispersion on the GA-based method, a series of THz pulses with different amounts of dispersion are simulated using a linear model, where the phase delay is proportional to frequency. Fig. 3 shows the simulated THz pulses that are modeled as Gaussians, where the dispersion parameter D increases from zero to 0.018π. In this model, the THz pulse is simulated by synthesizing it as a sum of 2500 harmonics, which is used to represent a bandwidth of 2.5 THz, with a spectral resolution of 1 GHz. A linear dispersion and a Gaussian spectral transfer function are then calculated for each harmonic in order to simulate the properties of the materials and measurement system. The harmonics are then summed to recreate the time-domain signal. As the dispersion D increases, the constituent harmonics are spread out in the time domain, as illustrated in Fig. 3(a)–(j). Fig. 4 demonstrates that the vector rejection parameter remains approximately flat as a function of dispersion—it is this property that we exploit to produce dispersion-independent classification.

By adding Gaussian white noise to these simulated signals with different SNR, labeled in Fig. 4, we evaluate the effect of noise on the λ parameter as a function of increasing dispersion.

IV. Materials and Methods

A. Sample Preparation

To verify the GA theory, four substances, melamine, tartaric acid, lactose, and glucose, are chosen for the experiment. All samples are purchased from the Sigma-Aldrich Corporation and used without further purification. In order to ensure that samples remain intact, each is mixed with HDPE powder in a mass ratio of 1:1. The resulting mixture is pressed into 13-mm-diameter tablets of five different thicknesses, 1.0, 1.5, 2.0, 2.5, and 3.0 mm. Each tablet is prepared by compressing the powders in a pellet press, and applying a pressure of 10 tonnes for 2 min.

B. THz Measurement System

The THz-TDS system consists of a Menlo 1560-nm T-Light fiber laser coupled to a photo-conductive antenna (PCA) transmitter, as well as a PCA receiver (model TERA15-TX/RX-FC). The laser produces 90-fs pulses at a repetition rate of 100 MHz. The THz transmitter and receiver utilize an InGaAs PCA manufactured by the Fraunhofer-Institut für Physikalische Messtechnik. The system is operated through TC-1550 control electronics for the laser head and an HVG110 electrical chopper for the emitter antenna. The signal is acquired with a lock-in amplifier with 16-bit data acquisition at 250 k-samples/s, connected to a PC with software for measurement and data analysis.

The THz radiation is free-space coupled to the sample with a spot waist size of 0.8-mm full width at half-maximum using a pair of broadband plano-convex TPX polymer lenses (model TPX50) with an effective focal length of 54 mm each. Another pair of lenses, of the same specification, is used to couple the THz radiation to the PCA receiver.

Each sample is placed in a custom-designed sample holder on an *X–Y* scanning harness consisting of a pair of Newport LTA-HZ actuators and translation stages. LabVIEW software is utilized to acquire the THz spectrum at each position, as the sample is moved in a 20×20 grid to acquire 400 separate measurements across the sample.

[1]The *vector rejection* is defined as the vector component orthogonal to the vector projection.

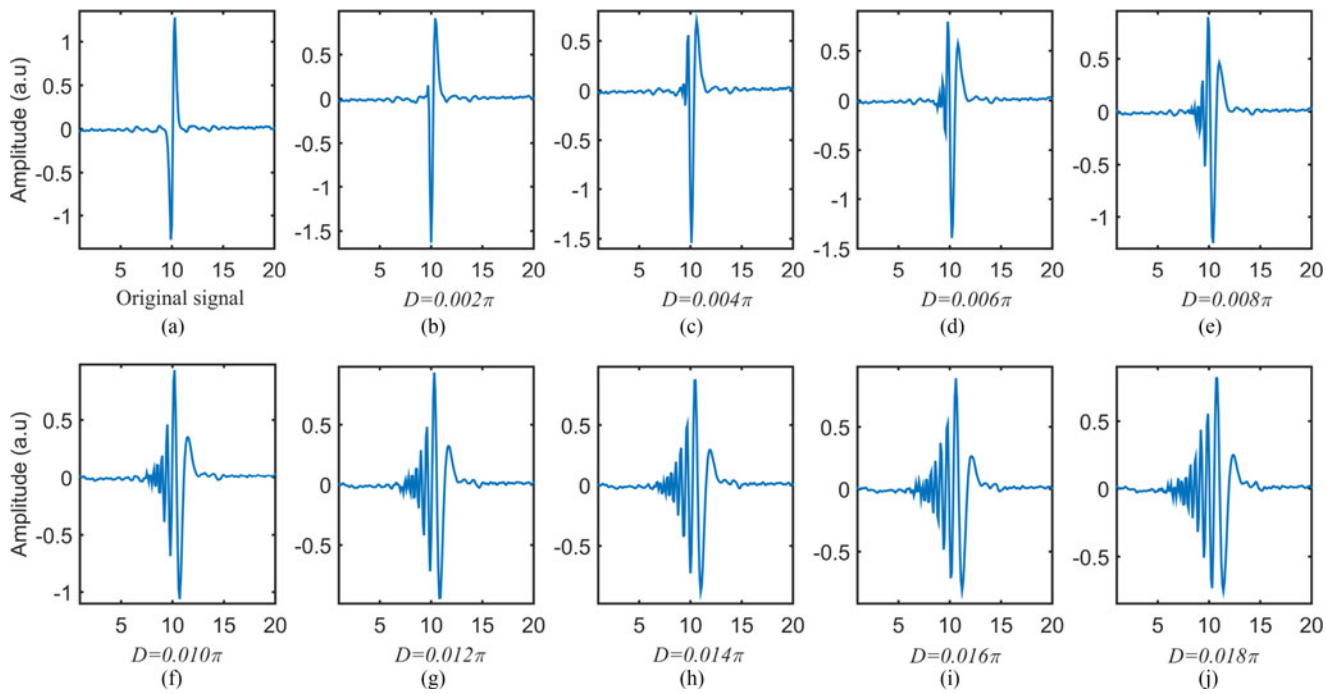

Fig. 3. Simulated THz pulses with different dispersion levels. (a) Simulated original THz signal without any dispersion. (b)–(j) Simulated THz signals with parameter D of 0.002π, 0.004π, 0.006π, 0.008π, 0.010π, 0.012π, 0.014π, 0.016π, and 0.018π.

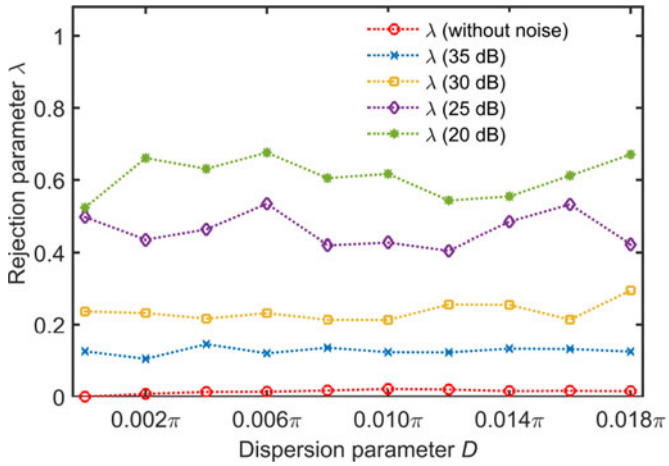

Fig. 4. The vector rejection parameter λ as a function of increasing dispersion, for simulated THz signals. The smaller the value of λ, the closer the signals are to the same plane. This plot shows that there is no obvious trend as dispersion increases. In the ideal case, with no noise, all signals are tightly bound to the same plane with $\lambda < 0.025$. In simulation, we see that as the SNR is progressively decreased to 20 dB, λ consequently increases.

C. THz Feature Extraction

Transfer functions $\tilde{h}(w)$ for all the investigated data samples are extracted by taking the Fourier transform after deconvolving measured time-domain signals with the reference signal, according to (2). To avoid the effects of noise, we select data from the 0.2–1.6-THz range for this equipment, where the signal stays well above the noise floor. The Fourier transform produces complex-valued spectra, containing both phase and magnitude information. Fig. 5(a)–(d) shows the amplitude spectrum of the transfer functions with a frequency in the range of 0.2–1.6 THz. Each is labeled by the corresponding thickness.

To verify the effectiveness of the proposed GA classifier, we carry out a comparison with the well-known multiclass SVM classifier. There are two kinds of datasets that are prepared separately for the SVM classifier and the GA classifier. For the GA classifier, by using (7) we calculate the GA vector $\boldsymbol{h}_i^{k,d}$ for every data sample i, where k denotes the substances melamine, tartaric acid, lactose, and glucose, each pressed into tablets of five different thicknesses, $d = 1.0$, 1.5, 2.0, 2.5, and 3.0 mm. For the SVM classifier, the amplitude spectra $\boldsymbol{a}_i^{k,d}$ of the substances are used as classification features, where $\boldsymbol{a} = |\boldsymbol{h}(w)|$.

D. Performance Assessment of Classification

In order to carry out a fair comparison between the SVM and GA classifiers, the same THz signals obtained from the 1.5- and 2.0-mm tablets are employed to train the SVM classifier and GA classifier separately. The classification process is as follows:

1) *Training Data Selection*: For each substance, 200 signals transmitted through a 1.5-mm pellet and 200 signals transmitted through a 2.0-mm pellet are randomly selected. Thus, the training set of 200 data samples equates to half the total size of 400 of each dataset.

2) *GA Classifier*: For each substance, we calculate their corresponding vectors, $\{\boldsymbol{h}_1^{k,d_1}\boldsymbol{h}_2^{k,d_1}, \boldsymbol{h}_3^{k,d_1}, \ldots, \boldsymbol{h}_{200}^{k,d_1}\}$ and $\{\boldsymbol{h}_1^{k,d_2}\boldsymbol{h}_2^{k,d_2}, \boldsymbol{h}_3^{k,d_2}, \ldots, \boldsymbol{h}_{200}^{k,d_2}\}$, and form the unit 2-blade H_k by using their average values as

$$\boldsymbol{H}_k = \frac{\boldsymbol{h}_k^{d_1} \wedge \boldsymbol{h}_k^{d_2}}{|\boldsymbol{h}_k^{d_1} \wedge \boldsymbol{h}_k^{d_2}|} \tag{16}$$

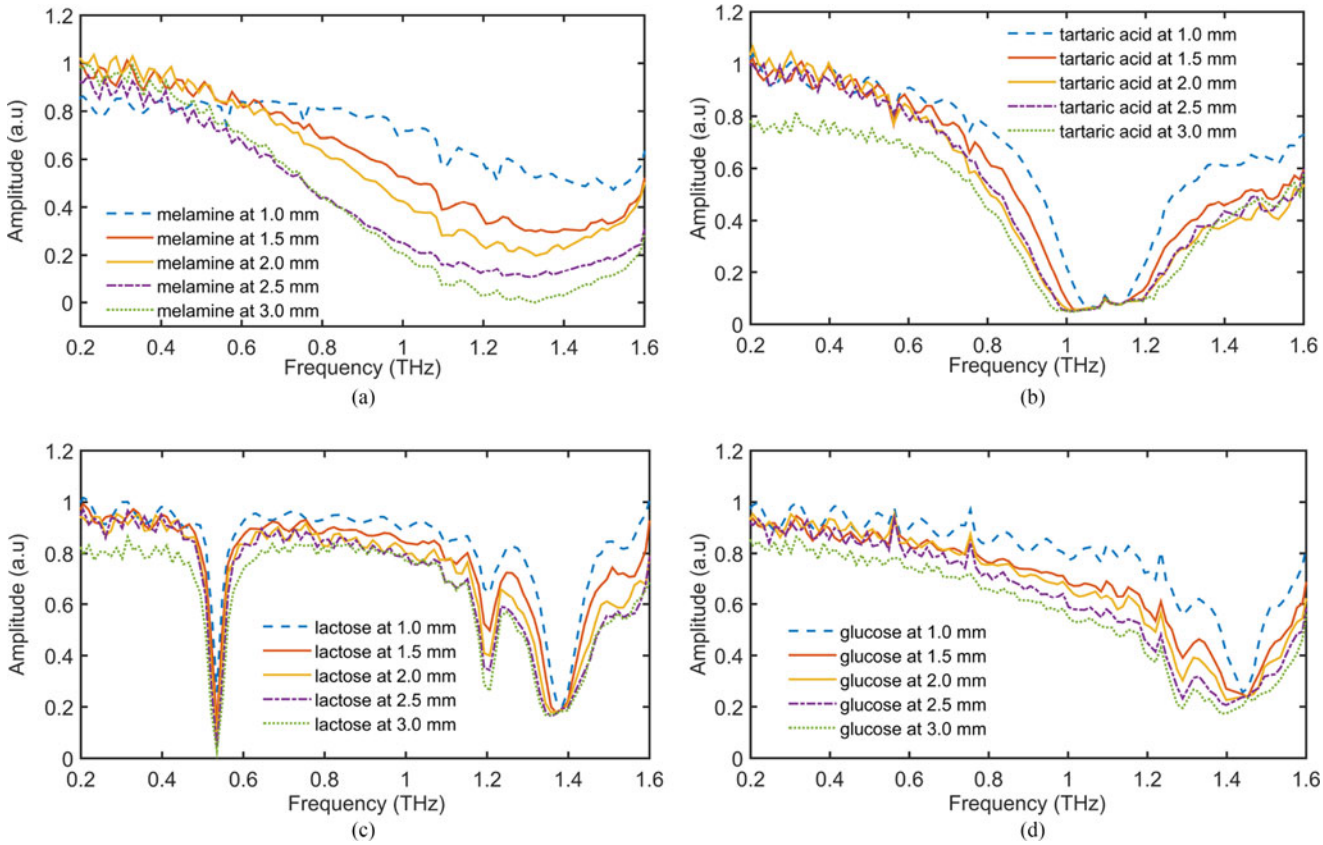

Fig. 5. Measurement of the average magnitude spectrum of four substances, melamine, tartaric acid, lactose, and glucose, at five different thicknesses. For each spectrum, the number of frequency samples is 104 corresponding to a 0.2–1.6-THz frequency range. The 2-blades associated with the four substances are calculated as the wedge product of vector pairs corresponding to the signals from the same substance at 1.5 and 2.0 mm.

where

$$\boldsymbol{h}_k^{d_1} = \frac{\boldsymbol{h}_1^{k,d_1} + \boldsymbol{h}_2^{k,d_1} + \boldsymbol{h}_3^{k,d_1} + \cdots + \boldsymbol{h}_{200}^{k,d_1}}{200} \tag{17}$$

$$\boldsymbol{h}_k^{d_2} = \frac{\boldsymbol{h}_1^{k,d_2} + \boldsymbol{h}_2^{k,d_2} + \boldsymbol{h}_3^{k,d_2} + \cdots + \boldsymbol{h}_{200}^{k,d_2}}{200} \tag{18}$$

$d_1 = 1.5$ mm and $d_2 = 2.0$ mm.

For any vector $\boldsymbol{h}_i^{x,d}$ corresponding to a signal from an unknown substance x with an unknown thickness d to be identified, we compute the value of λ_k^x, according to (14), which is used as the criterion in the substance identification. Here, λ_k^x denotes the magnitude of the vector rejection, for vector x, to the plane k. In other words, the closer the λ_k^x is to 0, the more likely the unknown substance x is the kth substance. Therefore, we can assume that the unknown is the kth substance, if the value of λ_k^x is smaller than for any of the other known substances.

3) *SVM Classifier*: In the classification process, all sample data are divided into three parts: 1) training set, 2) validation set, and 3) testing set. The selected 200 signals transmitted through 1.5-mm substances and 200 signals transmitted through 2.0-mm substances, their amplitude spectra, containing 104 frequency features, $\{\boldsymbol{a}_1^{k,d1}, \boldsymbol{a}_2^{k,d1}, \boldsymbol{a}_3^{k,d1}, \ldots, \boldsymbol{a}_{200}^{k,d1}\}$ and $\{\boldsymbol{a}_1^{k,d2}, \boldsymbol{a}_2^{k,d2}, \boldsymbol{a}_3^{k,d2}, \ldots, \boldsymbol{a}_{200}^{k,d2}\}$ are collected and normalized to make up the training set. Then, the amplitude spectra of the remaining 200 signals for 1.5- and 2.0-mm substance thicknesses are used as a validation set to determine classification accuracy. Finally, the remaining amplitude spectra for different thicknesses form the testing set.

In this paper, the statistics and machine learning toolbox of MATLAB are used to construct the SVM classifier. By use of a Gaussian kernel function, we map all features from a nonlinear feature space to a linear one, and the kernel scale and box constraint parameters are set to 8 and 2, respectively. In order to mitigate the overfitting problem and obtain the optional design of a multiclass SVM classifier, a five-fold cross-validation method is used for picking the most favorable parameters for the SVM classifier.

Once the SVM classifier is constructed, the validation set consisting of the amplitude spectra obtained from 1.5- and 2.0-mm substances is used to verify the performance of the SVM classifier. Then, this SVM classifier is applied to identify the resting amplitude spectra obtained from the 1.0-, 2.5-, and 3.0-mm samples.

4) *Comparison*: To further improve the estimate, steps 1 through 3 are repeated ten times. The accuracy values of the substance identification at a certain thickness over the ten runs are averaged to provide a statistical estimate of the classifier performance. These results are presented in Table I.

TABLE I
CLASSIFICATION PERFORMANCE (%) VERSUS SUBSTANCE THICKNESS USING SVM AND GA CLASSIFIERS

	SVM					GA				
Substances	1.0 mm	1.5 mm	2.0 mm	2.5 mm	3.0 mm	1.0 mm	1.5 mm	2.0 mm	2.5 mm	3.0 mm
Melamine	54.00	**100.00**	**100.00**	98.25	93.25	82.50	**97.75**	**100.00**	99.75	99.75
Tartaric acid	100.00	**100.00**	**100.00**	100.00	85.25	100.00	**99.75**	**99.75**	99.50	99.50
Lactose	99.00	**99.50**	**100.00**	99.00	62.70	99.75	**98.25**	**100.00**	100.00	100.00
Glucose	59.25	**100.00**	**100.00**	84.00	80.50	100.00	**97.50**	**97.75**	86.50	85.00
Overall	78.06	**99.87**	**100.00**	95.31	80.43	95.56	**98.31**	**99.37**	96.43	96.06

Bold columns indicate samples where half of the data points were used for training, and the other half used for identification.

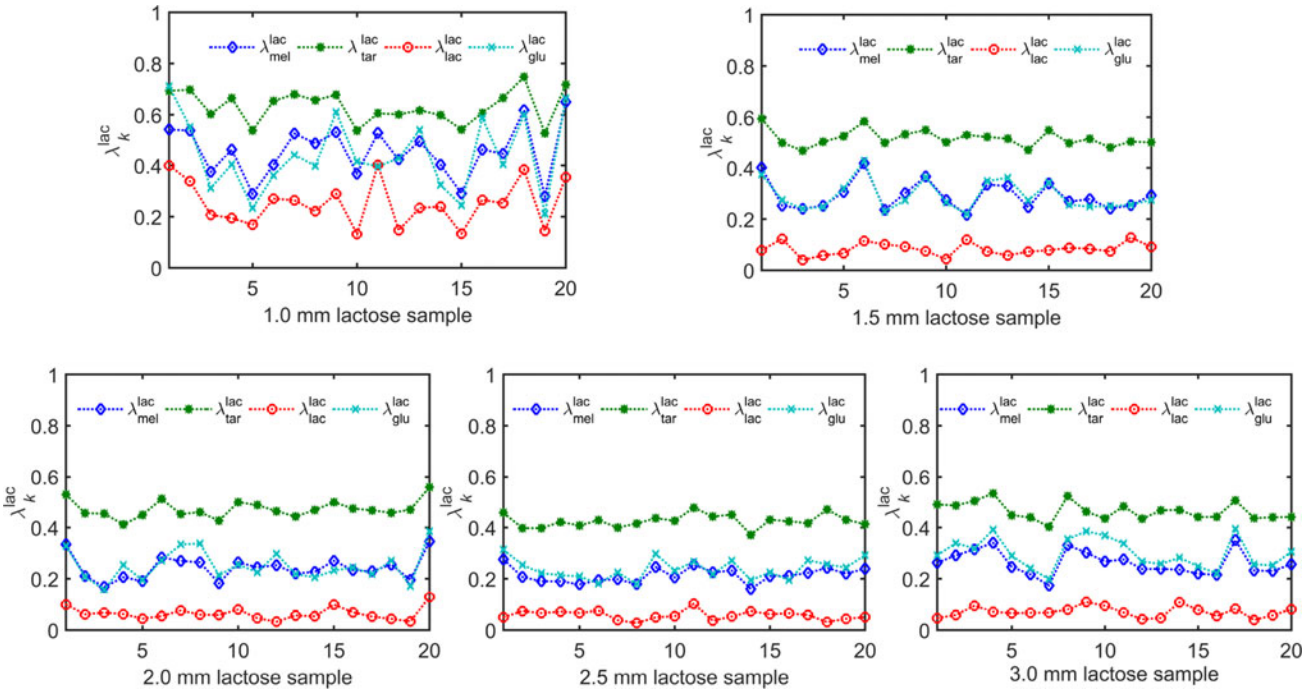

Fig. 6. Illustration of substance identification based on the GA classifier. Here, for purposes of illustration, 20 lactose vectors are randomly chosen from each dataset. Their magnitude rejections λ_k^{lac} to each plane are calculated using (14). Here, λ_k^{lac} denotes the magnitude of the lactose vector rejection to plane k, where k corresponds to four substances, melamine, tartaric acid, lactose, and glucose. In this graph, only the case of data from a 1.0-mm lactose sample is misclassified as glucose by the GA classifier.

E. Experimental Results Analysis

As shown in Fig. 5, the magnitude spectra for a given substance display increasing spectral broadening and greater influence of noise with increasing sample thickness. It is difficult to find an analytic expression to describe the relationship between the thickness and the magnitude spectrum. When the sample is relatively thin, the spectrum will be affected by etalon artifacts, as can be seen in the amplitude spectrum of the glucose at 1.0 mm. As the thickness increases, SNR rapidly falls off, and the effect of dispersion broadens the absorption spectra. Thus, a traditional classifier may not always work for an arbitrary sample thickness, if the classifier has been trained on data from a substance of one thickness.

Table I reports the classification outcomes of both the SVM classifier and the GA classifier for all four substances at thicknesses of 1.0, 1.5, 2.0, 2.5, and 3.0 mm. As can be seen from this table, for the SVM classifier trained on data from substances of thickness 1.5 and 2.0 mm, the overall classification accuracy is 99.87% for a substance thickness of 1.5 mm and 100% for a substance thickness of 2.0 mm. Notice that the overall classification accuracy of the SVM drops to as low as 78.06% for thicknesses that are outside the training set.

According to Theorem 3, the 2-blade defined by (13) determines a unique plane for each substance, which is independent of the thickness of each substance. In the ideal case, all GA vectors obtained from the same substance but with different thicknesses must be coplanar and lie on this plane. The inevitable influences of noise and other nonidealities in THz-TDS systems cause the GA vectors calculated from transfer functions to deviate from their real orientation, thus degrading the performance of the GA classifier. Clearly, our results show that these influences appear to affect the GA classifier to a lesser extent compared to the SVM classifier. As shown in Table I, the performance of the GA

classifier appears to be more consistent as a function of thickness, and the overall accuracy for all substances and thicknesses is always kept over 95%. Even in the worst case (melamine at 1.0 mm), the GA classification accuracy is still above 82.50%.

In GA theory, for any GA vector of an unknown substance x with an unknown thickness d, we compute the magnitude of each vector rejection to each plane according to (14), and choose the plane with a minimal λ value as its class label. So the classification standard of the GA classifier is a relative concept that results in an improved robustness. Taking lactose vectors, for example, Fig. 6 illustrates how the GA classifier works based on a minimal value of λ.

As we can see clearly from this graph, with a few exceptions, the magnitude of the vector rejections to the lactose plane is always minimal. For lactose vectors obtained from 1.5-, 2.0-, 2.5-, and 3.0-mm data samples, $\lambda_{\text{lac}}^{\text{lac}}$ remains about 0.1. For 1.0-mm lactose data samples, their vectors diverge more from their actual plane, and the magnitude of vector rejection to the lactose plane increases. However, from this graph, one can see that in most of the cases, the lactose plane has the lowest λ compared to the planes of the other substances. The GA classifier can still distinguish the spectra, which indicates the robustness and practicability of the GA classifier.

It is worth noting that by combining the advantages of signal preprocessing with classification, the prediction accuracy of the SVM classifier is likely to be improved, but the performance of the SVM classification model is influenced by many factors, including the features selected, the kernel function, kernel parameters, the training data, and data preprocessing techniques, and there are no specific guidelines to choose the kernel functions and set the value of the parameters for the SVM classifier. Previous studies have shown that no single kernel function or set of kernel parameters applies universally to any dataset to guarantee optimal classification performance [19]. On the other hand, the GA classifier is fundamentally different—it requires no training process, and its performance is less affected by external factors, rendering it potentially more reliable and practical.

V. Conclusion

Due to the presence of dispersion, noise, and other nonidealities, classification tasks were previously difficult to perform on samples having nonuniform thicknesses or unknown thicknesses. This may no longer be the case with the use of GA classifiers. In this paper, the THz transmitted signal is first analyzed on the basis of GA theory. It can be proved that the GA vectors obtained from the transfer function of samples of one substance but with different thicknesses are coplanar and belong to a unique plane. By analyzing the simulated THz signals with different levels of dispersion, it is confirmed that the substance identification based on the GA theory is independent of signal dispersion in the ideal noise-free case. Thus, a substance identification method independent of dispersion, via GA theory, is demonstrated. To validate the GA classifier, THz signals obtained from four substances of varying thicknesses are used for testing. The results confirm the superiority in classification accuracy and robustness of the GA classifier. It may also be concluded that the GA classifier is a powerful and less complex algorithm, without any tuning parameters.

This study now motivates future work to further validate the method on a diverse range of different datasets. The successful formulation of such a mathematical projection is not only of benefit for THz systems, but may also be suitable for other applications where pulsed time domain signals are involved, such as pulsed microwaves or even acoustic pulses through mechanical media or seismic pulses in geophysical systems.

Appendix

Proof of Theorem 1: For two substances, A and B, having exactly the same refractive index, $\tilde{\boldsymbol{n}}_A = \tilde{\boldsymbol{n}}_B$, $n_{Ai} = n_{Bi}$, and $\kappa_{Ai} = \kappa_{Bi}$, for $i = 1, 2, \ldots, m$. From the defining expression $\tilde{\alpha}_i = -\left(n_i - n_m + j\kappa_i\right)\frac{\omega_i}{c}, i = 1, 2, \ldots, m$, it is obvious that $\tilde{\boldsymbol{n}}_A = \tilde{\boldsymbol{n}}_B \Leftrightarrow \tilde{\boldsymbol{\alpha}}_A = \tilde{\boldsymbol{\alpha}}_B \Leftrightarrow \boldsymbol{\alpha}_A = \boldsymbol{\alpha}_B$. From the defining expression $\tilde{f}_i = \frac{4\tilde{n}_i n_m}{[\tilde{n}_i + n_m]^2}$, it follows that

$$\frac{4\tilde{n}_{Ai} n_m}{\left(\tilde{n}_{Ai} + n_m\right)^2} = \frac{4\tilde{n}_{Bi} n_m}{\left(\tilde{n}_{Bi} + n_m\right)^2}$$

when either $\tilde{n}_{Ai} = \tilde{n}_{Bi}$ or $\tilde{n}_{Ai}\tilde{n}_{Bi} = n_m^2, i = 1, 2, \ldots, m$. Assuming that for no two substances under investigation $\tilde{n}_{Ai}\tilde{n}_{Bi} = n_m^2$, it follows that $\tilde{\boldsymbol{n}}_A = \tilde{\boldsymbol{n}}_B \Leftrightarrow \tilde{\boldsymbol{f}}_A = \tilde{\boldsymbol{f}}_B \Leftrightarrow \boldsymbol{f}_A = \boldsymbol{f}_B$.

Proof of Theorem 2: For two substances, A and B, having exactly the same refractive index, $\tilde{\boldsymbol{n}}_A = \tilde{\boldsymbol{n}}_B$, it was shown that $\boldsymbol{f}_A = \boldsymbol{f}_B$ and $\boldsymbol{\alpha}_A = \boldsymbol{\alpha}_B$. Therefore, $\boldsymbol{f}_A \wedge \boldsymbol{f}_B = 0$ and $\boldsymbol{\alpha}_A \wedge \boldsymbol{\alpha}_B = 0$. Also, if for two substances, A and B, there exist nonzero real scalars λ_1 and λ_2, such that $\boldsymbol{f}_A = \lambda_1 \boldsymbol{f}_B$ and $\boldsymbol{\alpha}_A = \lambda_2 \boldsymbol{\alpha}_B$, then

$$\frac{\boldsymbol{f}_A \wedge \boldsymbol{\alpha}_A}{|\boldsymbol{f}_A \wedge \boldsymbol{\alpha}_A|} = \frac{\lambda_1 \boldsymbol{f}_B \wedge \lambda_2 \boldsymbol{\alpha}_B}{|\lambda_1 \boldsymbol{f}_B \wedge \lambda_2 \boldsymbol{\alpha}_B|} = \frac{\boldsymbol{f}_B \wedge \boldsymbol{\alpha}_B}{|\boldsymbol{f}_B \wedge \boldsymbol{\alpha}_B|}.$$

Proof of Theorem 3: Based on the properties of the wedge product, we have

$$\begin{aligned} \boldsymbol{h}_d \wedge \boldsymbol{H} &= (\boldsymbol{f} + d\boldsymbol{\alpha}) \wedge \boldsymbol{\alpha} \wedge \boldsymbol{f} \\ &= \boldsymbol{f} \wedge \boldsymbol{\alpha} \wedge \boldsymbol{f} + d\boldsymbol{\alpha} \wedge \boldsymbol{\alpha} \wedge \boldsymbol{f} \\ &= 0. \end{aligned}$$

References

[1] D. Abbott and X. C. Zhang, "Scanning the issue: T-ray imaging, sensing, and detection," *Proc. IEEE*, vol. 95, no. 8, pp. 1509–1513, Aug. 2007.

[2] W. Withayachumankul *et al.*, "T-ray sensing and imaging," *Proc. IEEE*, vol. 95, no. 8, pp. 1528–1558, Aug. 2007.

[3] X. X. Yin, B W.-H. Ng, and D. Abbott, *Terahertz Imaging for Biomedical Applications: Pattern Recognition and Tomographic Reconstruction.* New York, NY, USA: Springer, 2012.

[4] B. S.-Y. Ung *et al.*, "Dual-mode terahertz time-domain spectroscopy system," *IEEE Trans. THz Sci. Technol.*, vol. 3, no. 2, pp. 216–220, Mar. 2013.

[5] K. Kawase, Y. Ogawa, Y. Watanabe, and H. Inoue, "Non-destructive terahertz imaging of illicit drugs using spectral fingerprints," *Opt. Exp.*, vol. 11, pp. 2549–2554, 2003.

[6] B. Ferguson, S. Wang, D. Gray, D. Abbott, and X.-C. Zhang, "Identification of biological tissue using chirped probe THz imaging," *Microelectron. J.*, vol. 33, no. 12, pp. 1043–1051, 2002.

[7] N. Karpowicz *et al.*, "Comparison between pulsed terahertz time-domain imaging and continuous wave terahertz imaging,"*Semicond. Sci. Technol.*, vol. 20, no. 7, pp. S293–S299, 2005.

[8] Y. Zhao, W. Hong, and Y. Xu, "ECG beats feature extraction based on geometric algebra," in *Proc. Int. Conf. Comput. Intell. Softw. Eng.*, 2009, pp. 1–3.
[9] E. Hitzer, T. Nitta, and Y. Kuroe, "Applications of Clifford's geometric algebra," *Adv. Appl. Clifford Algebras*, vol. 23, no. 2, pp. 377–404, 2013.
[10] E. J. Bayro-Corrochano and N. Arana-Daniel, "Clifford support vector machines for classification, regression, and recurrence," *IEEE Trans. Neural Netw.*, vol. 21, no. 11, pp. 1731–1746, Nov. 2010.
[11] J. M. Chappell *et al.*, "Geometric algebra for electrical and electronic engineers," *Proc. IEEE*, vol. 102, no. 9, pp. 1340–1363, Sep. 2014.
[12] W. Xie, J. Li, and J. Pei, "THz-TDS signal analysis and substance identification," *J. Phys.: Conf. Ser.*, vol. 276, 2011, Art. no. 012227.
[13] X. X. Yin, B. W-H. Ng, B. M. Fischer, B. Ferguson, and D. Abbott, "Support vector machine applications in terahertz pulsed signals feature sets," *Sensors J.*, vol. 7, no. 12, pp. 1597–1608, 2007.
[14] G. Madzarov, D. Gjorgjevikj, and I. Chorbev, "A multi-class SVM classifier utilizing binary decision tree," *Informatica*, vol. 22, no. 2, pp. 233–241, 2009.
[15] E. Hitzer, T. Nitta, and Y. Kuroe, "Applications of Clifford's geometric algebra," *Adv. Appl. Clifford Algebras*, vol. 23, no. 2, pp. 377–404, 2013.
[16] D. Lundholm and L. Svensson, "Clifford algebra, geometric algebra, and applications," *Stockholm Arxivv1.d.mathematics Is Physics*, 2009.
[17] L. Dorst, S. Mann, and T. Bouma, "GABLE: A MATLAB tutorial for geometric algebra," 1999. [Online]. Available: http://carol. wins. uva. nl/leo/GABLE/i
[18] S. Mann, L. Dorst, and T. Bouma, "The making of a geometric algebra package in MATLAB," Univ. Waterloo, Waterloo, ON, Canada, Tech. Rep. CS-99-27, Dec. 1999. [Online]. Available: ftp://cs-archive.uwaterloo.ca/cs-archive/CS-99-27/
[19] C. C. Chang and C. J. Lin, "LIBSVM: A library for support vector machines," *ACM Trans. Intell. Syst. Technol.*, vol. 2, no. 3, pp. 1–27, 2011.

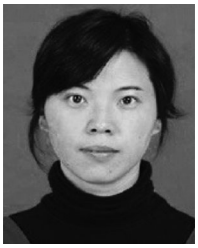

Shengling Zhou received the B.E. degree in metallurgical engineering and the M.E. degree in control science and engineering from Chongqing University, Chongquing, China, in 2003 and 2006, respectively. She embarked on the Ph.D. degree in agricultural engineering at Southwest University, Chongquing, China, in 2013.

Since 2008, she has been a Lecturer with Southwest University. In 2015, she won a China Scholarship Council (CSC) support as a Visiting Scholar under Tak W. Kee at The University of Adelaide, Adelaide, SA, Australia.

Dimitar G. Valchev received the M.Eng. degree in computer systems from the Technical University of Sofia, Sofia, Bulgaria, in 2001, and the Ph.D. degree in electrical engineering (in the area of communications and signal processing) from Northeastern University, Boston, MA, USA, in 2008.

He is currently an Assistant Professor with the Department of Computer Systems and Technologies, University of Food Technologies, Plovdiv, Bulgaria, and a Visiting Assistant Professor with the Institute of Optics, University of Rochester, NY, USA, under the 2015–2016 Fulbright Visiting Scholar Program of the U.S. Department of State. In 2014, he won a European Fellowship for early career researchers by the Group of Eight Australia for a collaborative visit at The University of Adelaide, SA, Australia, National T-ray Facility. In 2015, he won a fellowship by the Matsumae International Foundation for a collaborative visit at Nagoya University, Japan, Kawase Laboratory, for research on terahertz optics.

Alex Dinovitser (M'91) received the B.Eng. (Hons.) degree in electrical and computer systems engineering from Monash University, Melbourne, VIC, Australia, in 1991. He received the B.Sc. (Hons.) degree in physics in 2005, and was awarded a Ph.D. scholarship. He received the Ph.D. degree in physics from The University of Adelaide, Adelaide, SA, Australia, in 2012.

He has worked within the electronics manufacturing industry, designing computer interface and signal acquisition systems. His career then spanned from optical metrology to computer simulation modeling. In 2008, he built the first spectroscopic Lidar in Australia for the differential absorption detection of atmospheric trace gasses. Since 2013, he has been a Research Assistant with The National T-ray Facility, University of Adelaide.

Dr. Dinovitser is also a member of the Optical Society of America (OSA) and the Institution of Engineers (IEaust).

James M. Chappell received the B.E. degree (civil), Grad.Dip.Ed., B.Sc.(Hons.), and Ph.D. degrees from The University of Adelaide, Adelaide, SA, Australia, in 1984, 1993, 2006, and 2011, respectively.

During his Ph.D., he specialized in quantum computing and Clifford's geometric algebra. He began his career in civil engineering followed by employment as a Computer Programmer before retraining as a School Teacher. He is currently a Visiting Scholar with the School of Electrical and Electronic Engineering, The University of Adelaide, Adelaide, S.A., Australia, working on applications of geometric algebra.

Azhar Iqbal received the graduate degree in physics from the University of Sheffield, Sheffield, U.K., in 1995, and the Ph.D. degree in applied mathematics from the University of Hull, Hull, U.K., in 2006.

He received the Postdoctoral Research Fellowship for Foreign Researchers from the Japan Society for Promotion of Science to work under Prof. T. Cheon at the Kochi University of Technology, Japan, in 2006. In 2007, he received the prestigious Australian Postdoctoral Fellowship from the Australian Research Council, under D. Abbott, at the School of Electrical and Electronic Engineering, The University of Adelaide, Adelaide, SA, Australia. He is currently an Adjunct Senior Lecturer with the School of Electrical and Electronic Engineering, The University of Adelaide.

Brian Wai-Him Ng (S'97–M'02) was born in Hong Kong, on May 12, 1974. He received the B.Sc. degree in mathematics and computer science, and the B.Eng. (Hons.) degree and the Ph.D. degree, under A. Bouzerdoum, in electrical and electronic engineering from The University of Adelaide, Adelaide, SA, Australia, in 1996, 1997, and 2003, respectively.

Since 2002, he has been a Lecturer with the School of Electrical and Electronic Engineering, The University of Adelaide. His research interests include signal processing, bioinspired engineering, distributed sensor networks, software-defined radio, and signal processing for T-ray imaging.

Dr. Ng was the recipient of The University of Adelaide Medal for the Top Graduate in Electrical and Electronic Engineering.

Tak W. Kee received the B.S. degree in chemistry from Iowa State University, Ames, IA, USA, in 1997, where he received the Nelson Scholarship and the Felton Scholarship. In 2003, he received the Ph.D. degree in chemistry from the University of Texas, Austin, TX, USA.

During 2003–2006, he was a Postdoctoral Fellow with NIST, Gaithersburg, MD, USA. Since 2006, he has been with The University of Adelaide, Adelaide, SA, Australia, where he is currently an Associate Professor in chemistry.

Derek Abbott (M'85–SM'99–F'05) was born in South Kensington, London, U.K., in 1960. He received the B.Sc. (Hons.) degree in physics from Loughborough University, Leicestershire, U.K., in 1982, and the Ph.D. degree in electrical and electronic engineering from The University of Adelaide, Adelaide, SA, Australia, in 1995, under K. Eshraghian and B. R. Davis.

From 1978 to 1986, he was a Research Engineer with the GEC Hirst Research Centre, London, U.K. From 1986 to 1987, he was a VLSI Design Engineer with Austek Microsystems, Australia. Since 1987, he has been with The University of Adelaide, where he is currently a Full Professor with the School of Electrical and Electronic Engineering. He has authored or co-authored more than 800 publications and holds an equal number of patents. His research interests include multidisciplinary physics and electronic engineering applied to complex systems, networks, game theory, energy policy, stochastics, and biophotonics.

Dr. Abbott has been an invited speaker in more than 100 institutions. He coedited *Quantum Aspects of Life* (Imperial College Press, 2008), and coauthored *Stochastic Resonance* (Cambridge Univ. Press, 2008) and *Terahertz Imaging for Biomedical Applications* (Springer-Verlag, 2012). He is a Fellow of the Institute of Physics. He has been an Editor and/or Guest Editor for a number of journals, including the IEEE JOURNAL OF SOLID-STATE CIRCUITS, *Journal of Optics B, Microelectronics Journal, PLoS ONE*, PROCEEDINGS OF THE IEEE, and the IEEE PHOTONICS JOURNAL. He is currently on the Editorial Boards of IEEE ACCESS, Nature's *Scientific Reports*, *Royal Society Open Science*, and *Frontiers in Physics*. He was the recipient of a number of awards, including the South Australian Tall Poppy Award for Science (2004), the Premier's SA Great Award in Science and Technology for outstanding contributions to South Australia (2004), an Australian Research Council Future Fellowship (2012), and the David Dewhurst Medal (2015).